Benemérita Universidad Autónoma de Puebla

Facultad de Ciencias Físico Matemáticas

Estudio del diagrama de fase con dos sabores de QCD usando el modelo $3d\ O(4)$

Tesis presentada al

Posgrado en Física Aplicada

como requisito parcial para la obtención del grado de

Maestría en Ciencias (Física Aplicada)

por

Lic. Miguel Ángel Nava Blanco

asesorado por

Dr. Wolfgang Peter Bietenholz (ICN-UNAM)
Dr. Arturo Fernández Téllez (FCFM-BUAP)

Puebla Pue.
Diciembre 2018

Benemérita Universidad Autónoma de Puebla

Facultad de Ciencias Físico Matemáticas

Estudio del diagrama de fase con dos sabores de QCD usando el modelo $3d\ O(4)$

Tesis presentada al

Posgrado en Física Aplicada

como requisito parcial para la obtención del grado de

Maestría en Ciencias (Física Aplicada)

por

Lic. Miguel Ángel Nava Blanco

asesorado por

Dr. Wolfgang Peter Bietenholz (ICN-UNAM)
Dr. Arturo Fernández Téllez (FCFM-BUAP)

Puebla Pue.
Diciembre 2018

Título: Estudio del diagrama de fase con dos sabores de QCD usando el modelo $3d$ $O(4)$
Alumno: Lic. Miguel Ángel Nava Blanco

COMITÉ

Dra. Iraís Bautista Guzman
Presidente

Dr. Gilberto Tavares Velasco
Secretario

Dr. Justiniano Lorenzo Díaz Cruz
Vocal

Dr. Wolfgang Peter Bietenholz (ICN-UNAM)
Asesor

Dr. Arturo Fernández Téllez (FCFM-BUAP)
Asesor

FCFM-BUAP

Contents

Resumen

El diagrama de fase QCD es de interés desde varios puntos de vista. En cosmología, las transiciones de fase tuvieron lugar en el universo temprano. Las fases de alta temperatura de QCD también pueden realizarse en colisiones de iones pesados de energía suficientemente alta, es decir, en una pequeña región la fase a alta temperatura se obtiene y luego se enfría por medio de una transición de fase. Desde estas perspectivas, es importante comprender los fenómenos de las transiciones de fase apoyándose en las simetrías fundamentales y argumentos de universalidad y lo menos posible en suposiciones y modelos específicos.

En el límite quiral de 2 sabores de QCD, el parámetro de orden para la transición de fase quiral tiene la misma simetría que la magnetización de un imán de Heisenberg de cuatro componentes, una simetría $O(4)$, la cual lleva a cabo una transición de fase de segundo orden. Por lo tanto, esperamos que la simulación numérica del modelo σ no lineal en $3d$ con simetría global $O(4)$ proporcione una visión cualitativa del diagrama de fase QCD.

Abstract

The QCD phase diagram is of interest from several points of view. In cosmology, phase transitions took place in the early universe. High-temperature phases of QCD may also be realized in heavy ion collisions of sufficiently high energy, i.e., a small region of the high temperature phase is attained which then cools through a phase transition. From these perspectives, it is important to understand the phenomena of phase transitions, relying on fundamental symmetries and universality arguments and as little as possible on specific assumptions and models.

In the chiral limit of 2-flavor QCD the order parameter for the chiral phase transition has the same symmetry as the magnetization of a four component Heisenberg magnet, an O(4) symmetry, which performs a second order phase transition. So we hope that the numerical simulation of the $3d$ non-linear σ-model with a global $O(4)$ symmetry will provide qualitative insight into the QCD phase diagram.

Chapter 1

Introduction

1.1 Motivation

We know that water evaporates, then it can condense and rain over us in a cloudy day, but we know too that a solid piece of gold can be transformed in a beautiful necklace using heat and a good goldsmith. Phase transitions are an important part of our lives and even for the economy of countries, many materials have been studied to know their properties and their changes due several external factors as pressure or heat, and one of these materials that continue eluding a complete study of its properties and phase transitions is the elementary matter made by quarks.

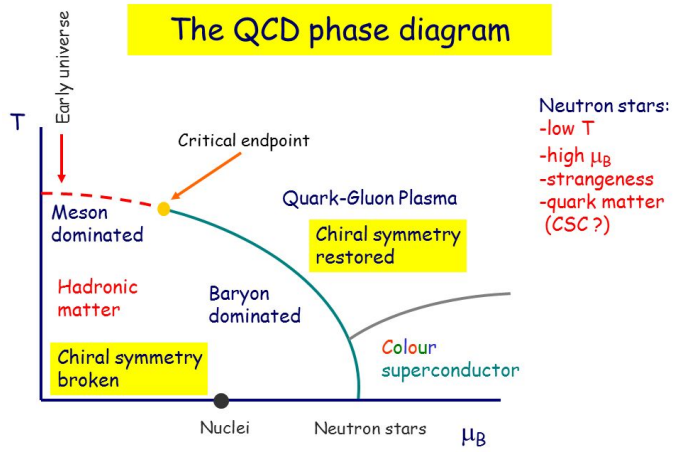

Figure 1.1: Hypothetical phase diagram.

The QCD phase diagram is one of the most prominent outstanding mysteries within the Standard Model of particle physics. A complete study of the QCD phase diagram using all the machinery is beyond the scope of this work. However, in our daily world we usually don't see heavy quarks as *top* and *bottom*, we can see that the ordinary matter is made by two light flavours, and that is the direction this work has taken.

This work will focus on the obtention of the phase diagram (as the one show in figure (1.1) using the non-linear σ $3d$ $O(4)$ model, which can be employed as a low-energy effective theory for the study of two massless QCD flavours. This effective model can be simulated on a lattice with a

powerful cluster algorithm which will allow us to identify the features of the critical temperatures from low to high baryon density. In this sense, this work will provide us with a conjecture about the phase diagram of QCD with two massless quark flavours.

This thesis begins with review of two main concepts to understand the phase transitions: the path integral formalism, the critical phenomena theory and their interconnection. With these tools a study of the non-linear σ $3d$ $O(4)$ model and its lattice regularisation is at hand for an effective low-energy nuclear physics model. After that the numerical results obtained from this model will be presented and a phase diagram will be given as a conclusion of this work.

1.2 Integral functional formalism

In the study of the elementary particles, quantum field theory is used, in special the formalism known as path integral formalism or integral functional. This formalism will be very useful in the study of the $3d$ $O(4)$ model, so a review of its basic properties will be useful.

In quantum mechanics the state of a system is described by $|\psi\rangle$ in a Hilbert space. If $|\psi(t)\rangle$ represents a state of the system in a time t and $|\psi(t')\rangle$ is a state of the system in a time t' $(t' \geq t)$ then exist an operator $\hat{U}(t',t)$ that connects both states of the system by

$$|\psi(t')\rangle = \hat{U}|\psi(t)\rangle, \tag{1.1}$$

where $\hat{U}(t',t)$ is the temporal evolution operator and satisfy the Schrödinger equation

$$i\hbar\frac{\partial}{\partial t'}\hat{U} = \hat{H}\hat{U}(t',t), \tag{1.2}$$

where $\hat{H}$ is the Hamiltonian of the system. If $\hat{H}$ does not depend on time then

$$\hat{U}(t',t) = \exp\big(-\frac{i}{\hbar}\hat{H}(t'-t)\big). \tag{1.3}$$

In the coordinate space the wave function is given by the scalar product $\psi(x,t) = \langle x|\psi(t)\rangle$, and at time t' it can be written as

$$\psi(x',t') = \int dx\langle x'|\hat{U}(t',t)|x\rangle\psi(x,t), \tag{1.4}$$

where the matrix element

$$\langle x'|\hat{U}(t',t)|x\rangle = \langle x'|\exp(-\frac{i}{\hbar}\hat{H}(t'-t))|x\rangle \tag{1.5}$$

is the propagator of the wave function.

If it is considered a time t_1 such as $t' \geq t_1 \geq t$ it can be obtained first the evolution of the system from t to t_1 and the from t_1 to t'

$$\langle x'|\hat{U}(t',t)|x\rangle = \langle x'|\exp(-\frac{i}{\hbar}\hat{H}(t'-t_1))\exp(-\frac{i}{\hbar}\hat{H}(t_1-t))|x\rangle, \tag{1.6}$$

or

$$\langle x'|\hat{U}(t',t)|x\rangle = \int dx_1\langle x'|\hat{U}(t',t_1)|x_1\rangle\langle x_1|\hat{U}(t_1,t)|x\rangle. \tag{1.7}$$

This last proceed can be generalized dividing the time interval $[t,t']$ in N equal parts

$$t'-t = N\epsilon \tag{1.8}$$

then inserting position eigenkets $|x_i\rangle$ in each intermediate time t_i

$$\langle x'|\hat{U}(t',t)|x\rangle = \int dx_1 \int dx_2 \cdots \int dx_{N-1} \langle x'|\hat{U}(t',t_{N-1})|x_{N-1}\rangle \cdots \times \langle x_1|\hat{U}(t_1,t)|x\rangle. \tag{1.9}$$

If the Hamiltonian is

$$\hat{H} = \frac{\hat{p}^2}{2m} + \hat{V}(\hat{x}), \tag{1.10}$$

then

$$\langle x_{i+1}|\hat{U}(t_{i+1},t_i)|x_i\rangle = \big(\frac{m}{2\pi\hbar\epsilon}\big)^{1/2} \exp\big[\frac{i\epsilon}{\hbar}\big(\frac{m}{2}\big(\frac{x_{i+1}-x_i}{\epsilon}\big)^2 - V(x_i)\big)\big], \tag{1.11}$$

so the propagator is

$$\langle x'|\hat{U}(t',t)|x\rangle = \int \mathcal{D}x \exp(\frac{i}{\hbar}S[x]), \tag{1.12}$$

where

$$S[x] = \lim_{\epsilon\to 0} \epsilon \sum_i \big[\frac{m}{2}\big(\big(\frac{x_{i+1}-x_i}{\epsilon}\big)^2 - V(x_i)\big)\big] = \int dt\big[\frac{m}{2}\dot{x} - V(x)\big], \tag{1.13}$$

and

$$\int \mathcal{D}x = \lim_{\epsilon\to 0} \big(\frac{m}{2\pi i\hbar\epsilon}\big)^{N/2} \int dx_1 \cdots \int dx_{N-1} \tag{1.14}$$

So equation (1.12) is about an integral over all the possible trajectories. Each integral $\int dx$ happens in a physical space, but the result is a sum over all the configurations.

This formalism is of a useful utility for the Quantum Field Theory (QFT) due it gives a bridge with statistical mechanics. Consider the partition function

$$Z = Tr \exp(-\beta\hat{H}), \tag{1.15}$$

where $\beta = 1/T$ and T is the temperature (with $k_B = 1$). If

$$\beta = \frac{i(t'-t)}{\hbar}, \tag{1.16}$$

(*Wick rotation*) then operator $\exp(-\beta\hat{H})$ in equation (1.15) corresponds with the evolution temporal operator (1.11). So a finite temperature can be identified with an imaginary time, the *eiclidian time*. Rotation of t in the complex plane by $\pi/2$ is called *Wick rotation*.

If an analog development of the eq. (1.12) is done but with the substitution ϵ by a in the Euclidean space, dividing the Euclidean time in N equal parts with

$$\beta = \frac{Na}{\hbar} \tag{1.17}$$

then it can be obtained the Euclidean path integral

$$Z = \int \mathcal{D}x \exp(\frac{-1}{\hbar}S_E[x]), \tag{1.18}$$

where

$$S_E[x] = \lim_{a\to 0} a \sum \big[\frac{m}{2}\big(\frac{x_{i+1}-x_i}{a}\big)^2 + V(x)\big] = \int_r^{t'} d\tau\big(\frac{m}{2}\dot{x}^2 + V(x)\big), \tag{1.19}$$

where

$$\int \mathcal{D}x = \lim_{a\to 0} \big(\frac{m}{2\pi\hbar a}\big)^{N/2} \int dx_1 \cdots \int dx_N. \tag{1.20}$$

Eq. (1.18) will be useful in the regularisation of the $3d$ $O(4)$ model.

1.3 Basics of the critical phenomena theory

Now that the connection between QFT and statistical mechanics has been revealed through the partition function in Euclidean time as given by eq. (1.18), a basic review of the critical phenomena theory will be welcomed.

A phase is a state of matter in which the macroscopic physical properties of the substance are uniform on a macroscopic length scale, e.g. 1 mm. Familiar examples are ice, liquid water, and water vapor. A phase is characterized by a thermodynamic function, typically the free energy which depends of few macroscopical parameters such as the temperature, pressure or density. A phase diagram is a graph with those parameters as the axes, on which the phase is specified for each point. A typical phase diagram has several specific features including phase boundaries and a critical points. A phase boundary separates different phases. A phase boundary sometimes disappears at a critical point, where the two phases become indistinguishable and the substance shows anomalous behavior. A phase can be characterized by various physical quantities. Especially important is the order parameter, which measures how microscopic elements constituting the macroscopic phase are ordered or in a similar state. the order parameter is associated with the breaking of a symmetry of the system under consideration. The order parameter measures the degree of asymmetry in the broken symmetry phase (which is the ordered phase), i.e. it is non-zero in the ordered phase and vanishes in the disordered phase.

A phase transition is a phenomenon in which a drastic change between thermodynamic phases occurs as the system parameters such as the temperature or density are varied. The characterization of a phase transition as a drastic change of macroscopic properties is described theoretically as the emergence of singularities (non-analyticities) in functions representing physical quantities, such as the specific heat c or magnetic susceptibility χ_m.

Phase transitions are roughly divided into two types by the degree of singularity in physical quantities. When the first-order derivative of the free energy F shows a discontinuity, the transition is of first order. The transition is called continuous if the second or higher-order derivatives of the free energy show a discontinuity or a divergence. It is common to name phase transitions by the order of the derivative that first shows a discontinuity or divergence, e.g. it is called second order if it is the second-order derivative of the free energy that first displays the discontinuity or divergence.

The connection between QFT and critical phenomena theory is now clearly visible through the integral path formalism that gives the partition function Z in Euclidean time [1] . A series of definitions follow to give an analytical method to the ideas of critical phenomena. For a quantity Q the expectation is defined as

$$\langle Q \rangle = \frac{1}{Z} \sum_i Q_i \exp(-\beta H_i). \tag{1.21}$$

For example, the expectation value of the energy $\langle H \rangle$ is given by

$$\langle H \rangle = \frac{1}{Z} \sum_i H_i \exp(-\beta H_i) = -\frac{\partial \log Z}{\partial \beta}. \tag{1.22}$$

The specific heat is given by

$$c = \frac{\partial U}{\partial T} = k_B \beta^2 \frac{\partial^2 \log Z}{\partial \beta^2} \tag{1.23}$$

Several quantities called *susceptibilities* will be used. In a general way, for two quantities X and Y, the susceptibility of X to Y measures the strength of the response of X to changes in Y and is usually defined as

$$\chi = \frac{\partial \langle X \rangle}{\partial Y} \tag{1.24}$$

[1] In d dimensional Euclidean space the action is given by $S_E = \int d^d x \mathcal{L}$ where $\mathcal{L}$ is the Lagrangian.

A deeper explanation can be found in ref. [1].

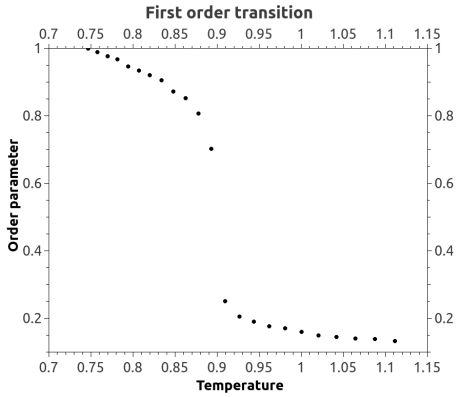

Figure 1.2: Typical plot from a first order transition. Observe the almost immediate fall around $T_{critical}$ in the order parameter.

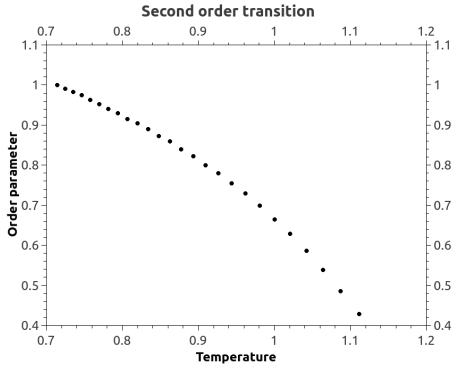

Figure 1.3: Typical plot from a second order transition. Observe the smooth fall in the order parameter as the temperature raises.

Chapter 2

$3d$ $O(4)$ model

2.1 Introduction

Particle physics is at heart of our understanding of the laws of nature. It is concerned with the fundamental constituents of the universe, the elementary particles and their interaction between them. In the atomic nucleus, the protons and neutrons are bound together by the strong nuclear force, which is a manifestation of the fundamental theory of strong interactions, called Quantum Chromodynamics (QCD).

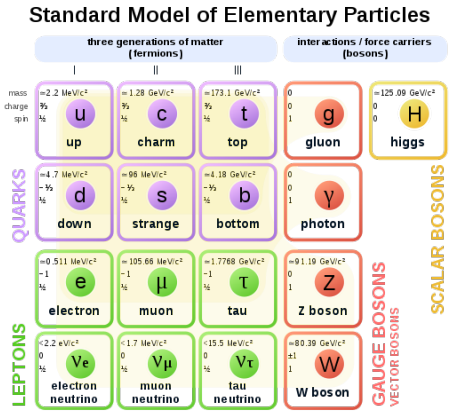

Figure 2.1: Particles conforming the Standard Model.

QCD provides a successful description of the strong interaction. It is formulated in terms of quarks and gluon fields that bound themselves in complex structures called hadrons. One distinguishes baryons (with valence three quarks inside) and mesons (pair quark-antiquark).

QCD has been tested since its development under several conditions, however, a question that is still open is the phase diagram and what happens at high baryon density. A non-trivial question if objects like neutron stars or the early universe are going to be studied in a comprehensive way.

One of the reasons why the phase diagram of QCD hasn't been settled yet by lattice simulations is the *sign problem*: Eq. (1.18) will be used to define a probability $p[U]$ that will be useful to generate configurations through Markov chains. However, the inclusion of the baryonic density μ_B will attach an imaginary part to the Euclidean action S_{QCD} that will turn the probability $p[U]$ in a complex number, so it will no longer define a probability and a straightforward approach to

simulate QCD as a statistical system fails.

Many attempts are being made to overcome this problem. One approach (and the one this work will focus on) to obtain a rough idea of what phases might occur is to use models that has some of the same properties as QCD, but are easier to manipulate. Now we proceed to find such a suitable model.

In particle physics is usual to work with natural units, which means that the values of $\hbar$ and c are fixed to 1 letting just one scale left ($[mass]$ for example) to describe the dimension of all quantities. With this in mind, if only massless quarks are used then the QCD Lagrangian does not involve any dimensional parameter which implies scale invariance at the classical level. At the quantum level, however, an intrinsic scale $\Lambda_{QCD} = 341(12)$ MeV emerges [2], which breaks this invariance.

In the real world, two flavours are very light compared to the intrinsic scale (see fig. 2.1). These two flavours dominate the low-energy nuclear physics which matters for our daily life. Then a sensible approximation is to consider only two massless flavours.

For N_f flavors of massless quarks there exist a (global) symmetry under chiral transformations in the group [6]

$$U(N_f)_L \otimes U(N_f)_R = SU(2)_L \otimes SU(2)_R \otimes U(1)_B \times U(1)_A. \tag{2.1}$$

of independent special unitary rotations of the left- and right- handed fields. Pat of this symmetry breaks explicitly due to quantum effects: in particular, the invariance under the group $U(1)_A = U(1)_{L\neq R}$ is broken by the axial anomaly [3]. Rotations with equal phases are captured by the symmetry group $U(1)_B = U(1)_{L=R}$ which corresponds to baryon number conservation. The remaining *chiral flavour symmetry* breaks spontaneously,

$$SU(N_f)_L \otimes SU(N_f)_R \to SU(N_f)_{L=R}, \tag{2.2}$$

which gives rise to N_f^2-1 Nambu-Goldstone bosons(NGB). The Goldstone bosons corresponding to the three broken generators are the three pions for $N_f = 2$. As a consequence, the effective theory of QCD bound states like the baryons, must now include mass terms for them, ostensibly disallowed by unbroken chiral symmetry. Thus, this chiral symmetry breaking induces the bulk of hadron masses, such as those for the nucleons — in effect, the bulk of the mass of all visible matter.

Chiral perturbation theory formulates a low-energy effective theory in terms of NGB fields[1] [4]: in this case its leading order Lagrangian reads (In Euclidean space)

$$\mathcal{L}(\partial_\mu U) = \frac{F_\pi^2}{4} Tr\left(\partial_\mu U \partial_\mu U^\dagger\right). \tag{2.3}$$

where $F_\pi^2 \simeq 92$ MeV is the pion decay constant.

At fixed Euclidean time x_4, the field U maps the 33d coordinate space to the group $SU(N_f)$. The identity $\Pi[SU(N_f)] = \mathbb{Z}$ implies that these maps are divided into topological sectors, labeled by a topological charge $Q \in \mathbb{Z}$. In this case, it is given by the term

$$Q = \frac{1}{24\pi^2} \int d^3x \epsilon_{ijk} Tr\left((U\partial_i U)(U\partial_j U)(U\partial_k U)\right), \quad i,j,k \in 1,2,3, \tag{2.4}$$

which is conserved in time. Topological charge Q can be interpreted as the *baryon number* [11]. For a comprehensive review see Ref. [12].

Actually the leading order Lagrangian (2.3) does not allow for stable semi-classical solution with $Q = 1$. In order to stabilize such a *skyrmion*, Skyrme added a four derivative term

$$\mathcal{L}_{Skyrme}(U, \partial_\mu U) = \frac{F_\pi^2}{4} Tr\left(\partial_\mu U \partial_\mu U^\dagger\right) + \frac{1}{32e^2} Tr\left[(\partial_\mu U^\dagger), (\partial_\nu U)U^\dagger\right]^2 \tag{2.5}$$

where e is a dimensionless parameter and the skyrmion represents a fermionic (bosonic) baryon [12].

[1] NGB fields $U(x) \in SU(N_f)$

2.2 The $3d$ $O(4)$ as a low-energy effective theory

For a simpler effective theory, the symmetry breaking pattern (2.2) can be describe by (locally) isomorphic orthogonal groups $O(N) \to O(n)$, $N > n$. This option is possible *solely* for $N_f = 2$ [13], where the transition (2.2) isomorphically corresponds to $O(4) \to O(3)$.

Therefore the $O(4)$ non-linear σ-model represents an effective theory for a low-energy QCD with $N_f = 2$ massless quark flavours. Its Euclidean action

$$S[\vec{S}] = \frac{F_\pi^2}{2} \int d^d x \partial_\mu \vec{s}(x) \cdot \partial_\mu \vec{s}(x), \qquad \vec{s}(x) \in S^3 \tag{2.6}$$

corresponds to the QCD low-energy Lagrangian for $N_f = 2$ massless quark flavours. The global $O(4)$ symmetry may break spontaneously down to $O(3)$, which yields three NGBs, with fields in the coset space $O(3)$, which is isomorphic to $SU(2)$.

As it can be seen, two flavour QCD is believed to belong to the the $3d$ $O(4)$ universality class at its chiral transition in the continuum limit (ref. [5]-[10]), so this work will focus in this model as a static Skyrme model. In this model, the configurations are divided into topological sectors, thus the skyrmions are present in this low-energy formulation as carriers of the baryon number [12]. Since these are topological properties, such a study must be non-perturbative.

2.3 Non-linear σ-models

The non-linear σ-models has some multi-component scalar field $\vec{s}(x)$, $\vec{s} = (s_1, s_2, \ldots, s_N) \in \mathbb{R}^2$, but now it is imposed — in each point x — the constraint $|\vec{s}(x)| = 1$. This kind of field is also denoted as a "classical spin".

Since the number 1 is dimensionless, the field $\vec{s}$ cannot have any dimension either, i.e. its dimension is $[mass]^0$. Therefore, the derivative term now requires a dimensioned factor. Indeed, Quantum Chromodynamics (QCD) at low energy can be expressed as an effective field theory ("Chiral Perturbation Theory") in this form, namely

$$L(\partial_\mu \vec{s}) = \frac{1}{2} F_\pi^2 \partial_\mu \vec{s}(x) \cdot \partial_\mu \vec{s}(x) \tag{2.7}$$

This term is a scalar product, and in Chiral Perturbation Theory for two massless quark flavours u and d, the field $\vec{s}$ $N = 4$ real-valued components. To get the dimension right, the factor F_π must have the dimension $[mass]^{(d-2)/2}$. In 4d QCD, it has a phenomenological meaning: it is known as the pion decay constant, which amounts to $F_\pi \approx 92$ MeV.

This is actually just the first term of the chiral expansion, but it already describes pion physics quite well. Even with this simple Lagrangian, its dynamics is complicated, exactly due to the constraint $|\vec{s}| = 1$ (otherwise it would be a trivial free theory).

If $\vec{s}$ has N components, then it lives on the unit sphere S^N in the N-dimensional spin space. The action is invariant when all spins are simultaneously rotated, i.e. when it is applied a global transformation $\vec{s}(x) \to \Omega \vec{s}(x)$, with an element of the orthogonal group, $\Omega \in O(N)$ (and therefore $\Omega^T = \Omega^{-1}$). Hence this type of model is also known as an $O(N)$ model.

Geometry tells that the field configurations fall into distinct topological sectors — which can be labeled by a topological charge (or winding number) $Q \in \mathbb{Z}$ — if the spin dimension exceeds the space-time dimension by 1, i.e. if $N = d + 1$. For this property to hold, it is assumed either $\vec{s}(x)$ to be constant at $|x| \to \infty$, or the system has a finite volume with periodic boundary conditions in all d directions.

The simplest example is the $1d$ $O(2)$ model: here $\vec{s}(t_E)$ is a point on the unit circle S^1, which moves as a function of the Euclidean time t_E. If this motion is continuous and periodic, then after a complete period, the point is back at its original position, and it has moved an integer number of times anti-clockwise around the circle (clockwise windings are counted negative). This net winding number is the topological charge $Q \in \mathcal{Z}$.

2.4 Dimensional reduction

Consider the system in a finite volume. It is convenient to assume periodic boundary conditions, since this provides translation invariance.

Assume the $4d$ volume to be of the form $\beta \times L^3$, where β is the extent in Euclidean time direction, and L is the side length of a spatial cube. Therefore the action reads

$$S_E[\vec{S}] = \frac{1}{2}F_\pi^2 \int_0^\beta dt_e \int_{L^3} d^3x \partial_\mu \vec{s} \cdot \partial_\mu \vec{s}, \tag{2.8}$$

where t_E is again the Euclidean time (here the square bracket indicates a functional of the field configuration).

In field theory, the inverse extent of the (periodic) Euclidean time corresponds to the temperature T of the system, $\beta = 1/T$. Consider the case of high T, where β is short. Assume it to be so short that in β-direction — for the statistically relevant field configurations — only the leading mode contributes significantly. All higher modes have a very high energy, so in this effective picture those modes decouple. Therefore the Lagrangian is (almost) *constant* in t_E, and the action can be approximated as

$$S_E[\vec{S}] = \frac{1}{2}F_\pi^2 \beta \int_{L^3} d^3x \partial_i \vec{s} \cdot \partial_i \vec{s}, \tag{2.9}$$

where $i = 1, 2, 3$ (in contrast to $\mu = 1, \ldots, 4$). Here β looks like an inverse coupling constant, but it also represents the inverse temperature (from the 4-dimensional perspective).

This simplification is called *dimensional reduction*. Note that this simplification takes this work to a 3-dimensional $O(4)$ model, which is endowed with topological charges. At this point, There might be some conflict with the assumption that the model is dealing with low energy, such that for instance the heavier quark flavours are negligible, and no higher terms (with 4 or more derivatives) are considered in the effective Lagrangian (2.7). Still, it is a reasonable assumptions to make sense.

2.5 Statistical mechanics and chemical potential

Now it is turn of Statistical Mechanics, which deals with an exponential of the form $\exp(-H/T)$. H is the Hamilton function, which is given by a spatial integral over the Hamilton density $\mathcal{H}$. In this case it can be identified by

$$H[\vec{S}] = \int d^3x \mathcal{H}, \qquad \mathcal{H} = \frac{1}{2}F_\pi^2 \partial_i \vec{s} \cdot \partial_i \vec{s}. \tag{2.10}$$

Clearly, H has dimension $[mass]$, and it can also be added a *chemical potential* μ_B. It multiplies the topological charge Q of a field configuration, which — in this effective low energy theory — represents the *baryon number*, as wise people like Skyrme and Witten pointed out,

$$H[\vec{S}] = \frac{1}{2}F_\pi^2 \partial_i \vec{s} \cdot \partial_i \vec{s} - \mu_B Q[\vec{S}] \tag{2.11}$$

The topological charge is an integer, $Q \in \mathbb{Z}$, and therefore dimensionless, while μ_B has dimension $[mass]$. It can be interpreted as the energy decrease if one baryon is added, or the energy that it takes to add an anti-baryon to the system.

2.6 Lattice regularisation

Calculations in QFT require an UV regularisation which preserves the symmetries. The lattice regularisation is a simple but powerful scheme: it reduces the Euclidean space to discrete sites x.

The most popular structure is a simple hyper-cubic lattice with spacing denoted as a. One often uses *lattice units* by setting $a = 1$ [14].

For the lattice regularisation (where it is instructive not to use lattice units) the lattice spacing a has dimension $[mass]^{-1}$. Now the field $\vec{s}_x$ is only defined on the lattice sites x, with $x/a \in \mathbb{Z}^3$. The derivative term is discretized in standard manner,

$$\partial_i \vec{s}(x) \to \frac{\vec{s}_{x+a\hat{i}} - \vec{s}_x}{a}, \tag{2.12}$$

where $\hat{i}$ is the unit 3-vector in the spatial direction of the component x_i. It is obtained

$$\partial_i \vec{s}(x) \cdot \partial_i \vec{s}(x) \to \frac{2}{a^2} \sum_i (1 - \vec{s}_{x+a\hat{i}} \cdot \vec{s}_x) \tag{2.13}$$

The additive constant is meaningless so it can be dropped (unless one is interested in gravity, where this would be a "cosmological constant"). Here only energy differences are taking in account, so the lattice Hamiltonian can be written in the familiar form (with $\int d^3x \to a^3 \sum_x$)

$$H_{lat}[\vec{S}] = -F_\pi a \sum_x \vec{s}_{x+a\hat{i}} \cdot \vec{s}_x - \mu_B Q[\vec{S}] \tag{2.14}$$

Denoting the inverse coupling that is used in the simulations as β_{lat}, the lattice action amounts to

$$S_{lat}[\vec{S}] = \beta_{lat} H_{lat}[\vec{S}] = \beta_{lat}\big(- \sum_x \vec{s}_{x+a\hat{i}} \cdot \vec{s}_x - \mu_{B,lat} Q[\vec{S}]\big). \tag{2.15}$$

Here the physical meaning of the dimensionless parameters are

$$\beta_{lat} = \beta F_\pi^2 a, \qquad \mu_{B,lat} = \frac{\mu_B}{F_\pi^2 a}. \tag{2.16}$$

2.7 Algorithm for the Monte Carlo simulation

Once a lattice field theory has been formulated, the original field theory problem becomes one of statistical mechanics: localize its critical points, the order of their transitions and the phase diagram. The goal of Monte Carlo method is to generate a sequence of configurations

$$[\vec{S}] \to [\vec{S}'] \to [\vec{S}''] \to \cdots . \tag{2.17}$$

Each new configuration is generated based on the previous one, without considering the earlier history[2].

To achieve this goal for the non-linear σ $3d$ $O(4)$ model and for $\mu_B = 0$ we consider the Hamilton function:

$$\mathcal{H} = - \sum_{\langle i,j \rangle} \vec{S}_i \cdot \vec{S}_j, \tag{2.18}$$

where $\langle ij \rangle$ means the nearest-neighbor sites on a three dimensional cubic lattice and $\vec{S}_i \in S^3$.

The Wolff single cluster algorithm is used due that for $O(N)$ models and this algorithm has proofed to be extremely efficient [17]:

1. Hot start: generate on each lattice site x independently a random spin $\vec{S}_x \in S^3$.

[2] This is called a *Markov chain*.

2. Choose randomly a spin $\vec{S}_1$ in the lattice. Call it "seed" and attach it to the cluster.

3. Generate a random 4-component unit vector $\vec{r}$ and define the reflection with respect to the 3d hyperplane orthogonal to $\vec{r}$ as:

$$R(\vec{r})\vec{S_x} = \vec{S_x} - 2(\vec{S_x} \cdot \vec{r})\vec{r}. \tag{2.19}$$

4. Consider the nearest neighbors of the seed, $\vec{s_2}$ for example:

   - If $\Delta H = H[\vec{S}_1, R(\vec{S_2})] - H[\vec{S}_1, \vec{S_2}] < 0$ then do not attach $\vec{s_2}$ to the cluster.
   - If $\Delta H = H[\vec{S}_1, R(\vec{S_2})] - H[\vec{S}_1, \vec{S_2}] > 0$ then attach $\vec{s_2}$ to the cluster with probability $P = 1 - \exp(-\beta \Delta H)$.

5. Repeat the same steps with all the neighbors of the seed and with the neighbors of the spins added to the cluster, until the cluster does not grow anymore.

6. Apply the reflection defined in step 3 to all spins in the cluster.

To a comprehensive study of the Wolff cluster algorithm see references [1] and [17].
If it is considered the model with $\mu_B > 0$ then eq. (2.18) is replaced by

$$\mathcal{H} = -\sum_{\langle ij \rangle} \vec{S}_i \cdot \vec{S}_j - \mu_B Q[\vec{S}], \tag{2.20}$$

where μ_B is the baryonic chemical density and $Q[\vec{S}]$ is the topological charge of the configuration $\vec{S}$. To include the effect of $\mu_B > 0$ to the Monte Carlo it is suggested to proceed as follow:

1. Build the single cluster using the Wolff algorithm without considering the new term.

2. Compute the charge Q for the present configuration, $Q[\vec{S}]$, and for the configuration which would emerge when this flip is performed, $Q[\vec{S}']$.

3. Perform a *Metropolis* accept/reject step to decide if flip the cluster or not assuming $\mu_B > 0$.

Where the *Metropolis* step is:

- If the flip decreases Q, flip the cluster.
- If the flip increases Q, flip the cluster with probability $p = \exp(-\beta \mu_B (Q[\vec{S}'] - Q[\vec{S}]))$

In practice, one first performs the thermalization, and one fixes empirically a number N_{steps} of sweeps between the measurements. This number must be sufficient to make the measurements statistically independent, which can be checked by the auto-correlation or (simpler) by numerical experiments with different N_{steps} : if increasing it doesn't change the results (within errors), then it is large enough (the same applies to the number of thermalization sweeps).

After thermalization, thermodynamic quantities like eqs. (1.21)-(1.24) can be measured and important conclusions can be retrieved [15].

Chapter 3

Numerical results for the $3d$ $O(4)$ model

3.1 Topological charge

The geometric definition of the topological charge has been successfully applied in the $2d$ $O(3)$ model [18]. In order to extend the geometric definition of Q for the $3d$ $O(4)$ model, all the lattice unit cubes are decomposed in six tetrahedra (see figure 3.1). For a given tetrahedron, the spin variables $\vec{S}_1$, $\vec{S}_2$, $\vec{S}_3$ and $\vec{S}_4$ span a *spherical tetrahedron* on the 3-dimensional sphere S^3.

For a given lattice configuration in some volume V with periodic boundaries conditions, lattice unit cubes are split into tetrahedra, and all volumes of the corresponding oriented spherical tetrahedra are summed up to obtain the topological charge $Q \in \mathbb{Z}$. It counts how many times the sum of the spherical tetrahedra covers the sphere S^3 and represent the baryon number in this low energy effective model [12].

Steps for the calculation of the topological charge:

1. Lattice is divided in cubic units. Each cubic unit has a six tetrahedron ordered structure: [F,H,A,E],[G,B,F,H],[H,A,B,F],[H,G,B,D],[A,B,D,H],[G,B,D,C].

2. From the four spins in the edge of each tetrahedron, the signed volume of the spherical tetrahedron in $\mathbb{R}^4$ formed for these four spins is calculated.

3. All the signed volumes of all the spherical tetrahedron from all the lattice units are summed and divided by $2 \times \pi^2$, the volume of S^3. The result is the topological charge Q.

The calculation of the volume of the spherical tetrahedra can be computed according to the formulae elaborated only recently in Ref. [19]. For the calculation of the volume of a spherical tetrahedron spanned by the four spins it was used **theorem 1.2** from ref. [19].

Theorem 1. *Let T be a spherical tetrahedron with edge lengths $l_1, l_2, ..., l_6$ at the edges $e_1, e_2, ..., e_6$ respectively given in figure 3.1 . Let $b_j = e^{il_j}$ for $j = 1, 2, ..., 6$ and*

$\widetilde{L}(b_1, b_2, b_3, b_4, b_5, b_6, z) = L(-b_4^{-1}, -b_5^{-1}, -b_6^{-1}, -b_1^{-1}, -b_2^{-1}, -b_3^{-1}, z)$. Then the following formula holds.

For a spherical tetrahedron T as above,

$$Vol(T) = Re(\widetilde{L}(b_1, b_2, ..., \widetilde{z_0})) - arg(-\widetilde{q_2})\pi - \sum_{j=1}^{6} l_j \frac{\partial Re(\widetilde{L}(b_1, b_2, ..., b_6, z))}{\partial l_j}\Big|_{z=\widetilde{z_0}} - \frac{1}{2}\pi^2 \quad mod\ 2\pi^2, \tag{3.1}$$

where $\widetilde{z_0}$ and $\widetilde{q_2}$ are obtained from z_0 and q_2 given in ref. [19] by substituting $-b_{j\pm3}^{-1}$ to a_j for $j = 1, 2, ..., 6$.

The notation in theorem (1) was changed to a better understanding of the one. **Edge length** is the linear distance between two spins $\vec{S_i}$ and $\vec{S_j}$. **Spherical edge length** is the arc of a circle of radius 1 with $\vec{S_i}$ and $\vec{S_j}$ as vertices.

An strange point that was found in the calculation of the spherical tetrahedron volume is that the order of the edge lengths e_i's matters in Murakami's formula, so the next agreement was reached: In the calculation of the volume of the spherical tetrahedron formed by four spins $\vec{S}_1$, $\vec{S}_2$, $\vec{S}_3$ and $\vec{S}_4$, the spin $\vec{S}_1$ is the top corner of the spherical tetrahedron, $\vec{S}_2$ will be the left corner, $\vec{S}_3$ is the one at the bottom and $\vec{S}_4$ will be the corner at the right, so then the edge length e_1 connects $(\vec{S}_1, \vec{S}_2$, e_2 connects $(\vec{S}_1, \vec{S}_3)$, e_3 connects $(\vec{S}_1, \vec{S}_4)$, e_4 connects $(\vec{S}_3, \vec{S}_4)$, e_5 connects $(\vec{S}_2, \vec{S}_4)$ and e_6 connects $(\vec{S}_2, \vec{S}_3)$. The vectors were fixed that way because it seemed to match the order given in ref. [19] (see figure 3.1).

For the determination of the volume the next quantities are used:

$$q_0 = a_1a_4 + a_2a_5 + a_3a_6 + a_1a_2a_6 + a_1a_3a_5 + a_2a_3a_4 + a_4a_5a_6 + a_1a_2a_3a_4a_5a_6 \tag{3.2}$$

$$q_1 = -(a_1 - a_1^{-1})(a_4 - a_4^{-1}) - (a_2 - a_2^{-1})(a_5 - a_5^{-1}) - (a_3 - a_3^{-1})(a_6 - a_6^{-1}) \tag{3.3}$$

$$\begin{aligned} q_2 = {} & a_1^{-1}a_4^{-1} + a_2^{-1}a_5^{-1} + a_3^{-1}a_6^{-1} + a_1^{-1}a_2^{-1}a_6^{-1}) + a_1^{-1}a_3^{-1}a_5^{-1} \\ & + a_2^{-1}a_3^{-1}a_4^{-1} + a_4^{-1}a_5^{-1}a_6^{-1} + a_1^{-1}a_2^{-1}a_3^{-1}a_4^{-1}a_5^{-1}a_6^{-1} \end{aligned} \tag{3.4}$$

$$z_0 = \frac{-q_1 + \sqrt{q_1^2 - 4q_0q_2}}{2q_2} \tag{3.5}$$

$$\begin{aligned} L(a_1, a_2, ..., a_6, z) = {} & \frac{1}{2}(Li_2(z) + Li_2(a_1^{-1}a_2^{-1}a_4^{-1}a_5^{-1}z) + Li_2(a_1^{-1}a_3^{-1}a_4^{-1}a_6^{-1}z) \\ & + Li_2(a_2^{-1}a_3^{-1}a_5^{-1}a_6^{-1}z) - Li_2(-a_1^{-1}a_2^{-1}a_3^{-1}z) - Li_2(-a_1^{-1}a_5^{-1}a_6^{-1}z) \\ & - Li_2(-a_2^{-1}a_4^{-1}a_6^{-1}z) - Li_2(-a_3^{-1}a_4^{-1}a_5^{-1}z) \\ & + \log a_1 \log a_4 + \log a_2 \log a_5 + \log a_3 \log a_6) \end{aligned} \tag{3.6}$$

For the treatment of the dilogarithm functions it may be expand the logarithm in powers of z, obtaining the Taylor series expansion for the dilogarithm, valid for $|z| \leq 1$,

$$Li_2(x) = -\int_0^x \frac{\log(1-t)}{t} dt \qquad \Rightarrow \qquad Li_2 = \sum_{k=1}^{\infty} \frac{z^k}{k^2}. \tag{3.7}$$

A complete study of dilogarithm function can be found at ref. [20].

The signed volume of the spherical tetrahedron formed by $\vec{S}_1$, $\vec{S}_2$, $\vec{S}_3$ and $\vec{S}_4$ is given by

$$V(\vec{S}_1, \vec{S}_2, \vec{S}_3, \vec{S}_4) = sign(det(\vec{S}_1, \vec{S}_2, \vec{S}_3, \vec{S}_4)) \times Vol(\vec{S}_1, \vec{S}_2, \vec{S}_3, \vec{S}_4) \tag{3.8}$$

3.2 Set-up

The next results for the $3d$ $O(4)$ model were obtained with the single cluster Wolff algorithm (for the formation of clusters) and Metropolis algorithm (for the acceptance of the clusters) with several baryonic chemical potentials ($\mu_B \geq 0$).

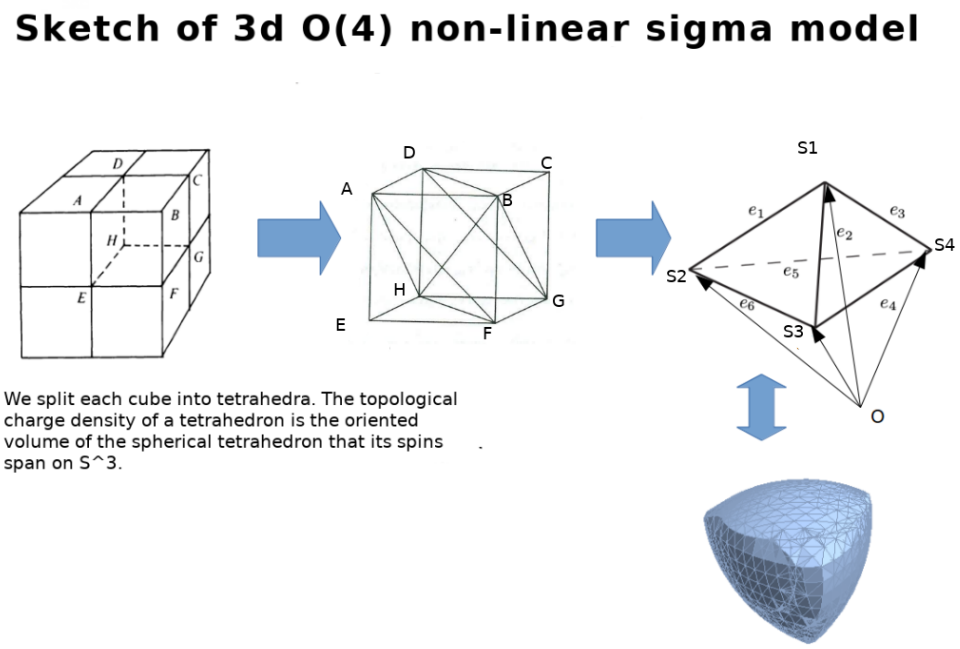

Figure 3.1: Sketch for the calculation of the topological charge for the $3d$ $O(4)$ model.

In all the cases, the lattice structure and volume is cubic, $V = L^3$, with periodic conditions in all directions.

We denote the spin field as $\vec{S}_x$, with $|\vec{S}_x| = 1$ and $\vec{S}_x = (s_1, s_2, s_3, s_4)$ and we use the lattice action and Hamiltonian function

$$S[\vec{S}] = \beta H[\vec{S}], \qquad H[\vec{S}] = -\sum_{\langle xy \rangle} \vec{S}_x \cdot \vec{S}_y - \mu_B Q[\vec{S}], \tag{3.9}$$

where $\langle xy \rangle$ are nearest-neighbor lattice sites, β is interpreted as the inverse of the temperature, μ_B is the baryonic chemical density and $Q[\vec{S}]$ is the topological charge of the configuration $\vec{S}$.

For the thermodynamic quantities the following definitions are referred:

Topological susceptibility $$\chi_t = \frac{\langle Q^2 \rangle - \langle Q \rangle^2}{V},$$

Specific heat $$c = \frac{\beta^2}{V}(\langle \mathcal{H}^2 \rangle - \langle \mathcal{H} \rangle^2)$$

Magnetization $$\vec{M} = \sum_x \vec{S}_x$$

Magnetic susceptibility $$\chi_m = \frac{\beta}{V}(\langle M^2 \rangle - \langle |M| \rangle^2).$$

In addition to those quantities, the correlation function $C(r)$ is also measured, given by

$$C(r) = \langle \vec{S}_{x3} \cdot \vec{S}_{x3+r} \rangle \propto \cosh\Big(\frac{r - L/2}{\xi}\Big),$$

where ξ is the correlation length and $\vec{S}_{x3} = \frac{1}{L^2} \sum_{x1,x2} \vec{S}_x$.

The second moment correlation length is

$$\xi_2 = \Big(\frac{(\chi_m/\mathcal{F}) - 1}{4\sin^2(\pi/L)}\Big)^{1/2},$$

where

$$\mathcal{F} = \frac{1}{V} \sum_{x,y} \langle \vec{S}_x \cdot \vec{S}_y \rangle \cos\Big(\frac{2\pi(x_1 - y_1)}{L}\Big).$$

For the calculation of the topological charge a change in the algorithm is used to speed-up the code: In place of calculating the volume of the spherical tetrahedron, a random spin $\vec{r}$ is used and if this spin is inside the spherical tetrahedron formed by $\vec{S}_1$, $\vec{S}_2$, $\vec{S}_3$ and $\vec{S}_4$, then $dQ = \pm 1$ (depending of the orientation of $\vec{S}_1$, $\vec{S}_2$, $\vec{S}_3$ and $\vec{S}_4$) or $dQ = 0$ if $\vec{r}$ is not inside the spherical tetrahedron. dQ_i's are calculated through all the lattice cubic units and summed up, so

$$Q = \sum_i dQ_i. \tag{3.10}$$

If all the components of $\vec{T}$ are positive in eq. (3.11) then $\vec{r}$ is inside the spherical tetrahedron formed by $\vec{S}_1$, $\vec{S}_2$, $\vec{S}_3$ and $\vec{S}_4$.

$$\vec{r} = [\vec{S}_1 \vec{S}_2 \vec{S}_3 \vec{S}_4]\vec{T}. \tag{3.11}$$

This algorithm is in agreement with the usual way to get the topological charge, but it is much faster.

3.3 Numerical results for lattices with $V = 8^3$

For the single-cluster algorithm, a *sweep* is defined as follows: After thermalisation, n_1 measurements of cluster sizes separated by $10 \times V$ single-cluster steps are made. A *sweep* is defined as

$$sweep = \frac{V}{\langle cluster \rangle},$$

where $\langle cluster \rangle$ is the mean of n_1 cluster sizes after the thermalization of the system separated by $10 \times V$.

The definition of *sweep* is used to speed-up the gathering of data. Table 3.1 shows the statistics involved.

Figure 3.2 shows the behavior of the cluster size under two different $\beta = 0.7, 1.5$ and $\mu_B = 0.0$. A $L = 8$ lattice is used.

Figure 3.3 shows the behavior of the topological susceptibility.

The four graphs from figure 3.4 shows the behavior of the specific heat c as function of β_c as the baryonic chemical density is raised using lattices of volume $V = 8^3$. From critical phenomena theory it is known that c diverges at β_c.

Figure 3.5 shows the behavior of the magnetic susceptibility. Magnetic susceptibility diverges at β_c.

Figure 3.6 shows the behavior of $\langle |M| \rangle$, it is the so called order parameter and, from critical phenomena theory, it gives the order of the transition phase.

Thermalisation	n_1	N_{data}
$1000 \times V$	2000	15000

Tabla 3.1: Statistics of the simulations: The systems begins in a "hot start" and takes $1000 \times V$ steps to thermalise it, then n_1 cluster size are measured separated by $10 \times V$ steps and *sweep* is calculated. After that, N_{data} measurements are made separated by $10 \times sweep$ steps.

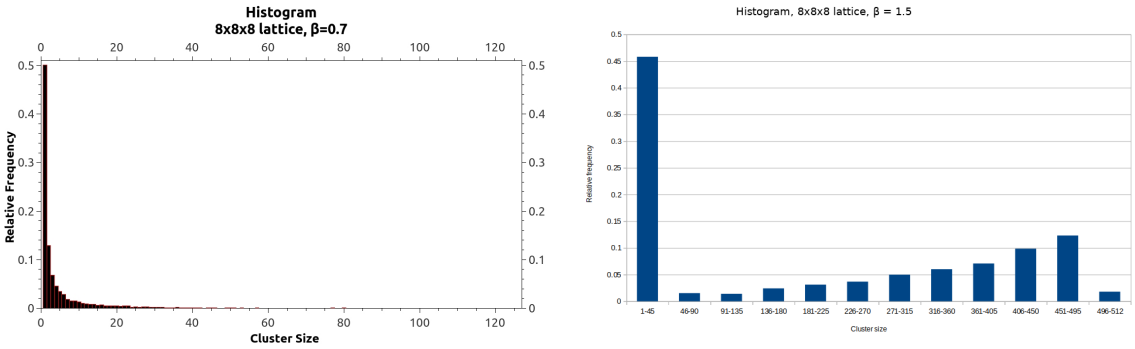

Figure 3.2: Behavior of the cluster sizes after thermalisation for $\beta = 0.7$, $\beta = 1.5$, $\mu_B = 0$ and using $L = 8$. The distributions shows larger clusters for $\beta = 1.5$ as expected.

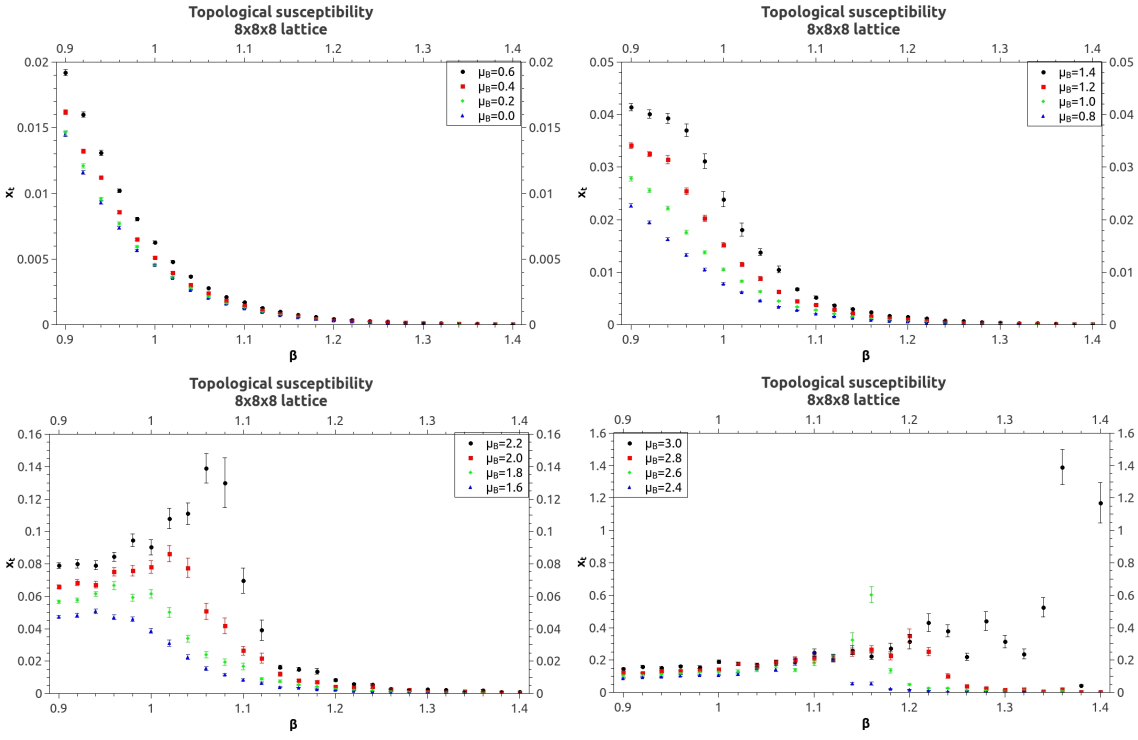

Figure 3.3: Behavior of the topological susceptibility χ_t under several μ_B. At $\mu_B = 0$, $\langle Q \rangle$ must be zero due to parity invariance, and at large β, there are only few top. windings, which are exponentially suppressed, as one expects for a dilute instanton gas. It can be seen too that $\langle Q \rangle$ decreases with larger μ_B, but increases with larger β, until at high T the effect of μ_B is washed out be strong fluctuations.

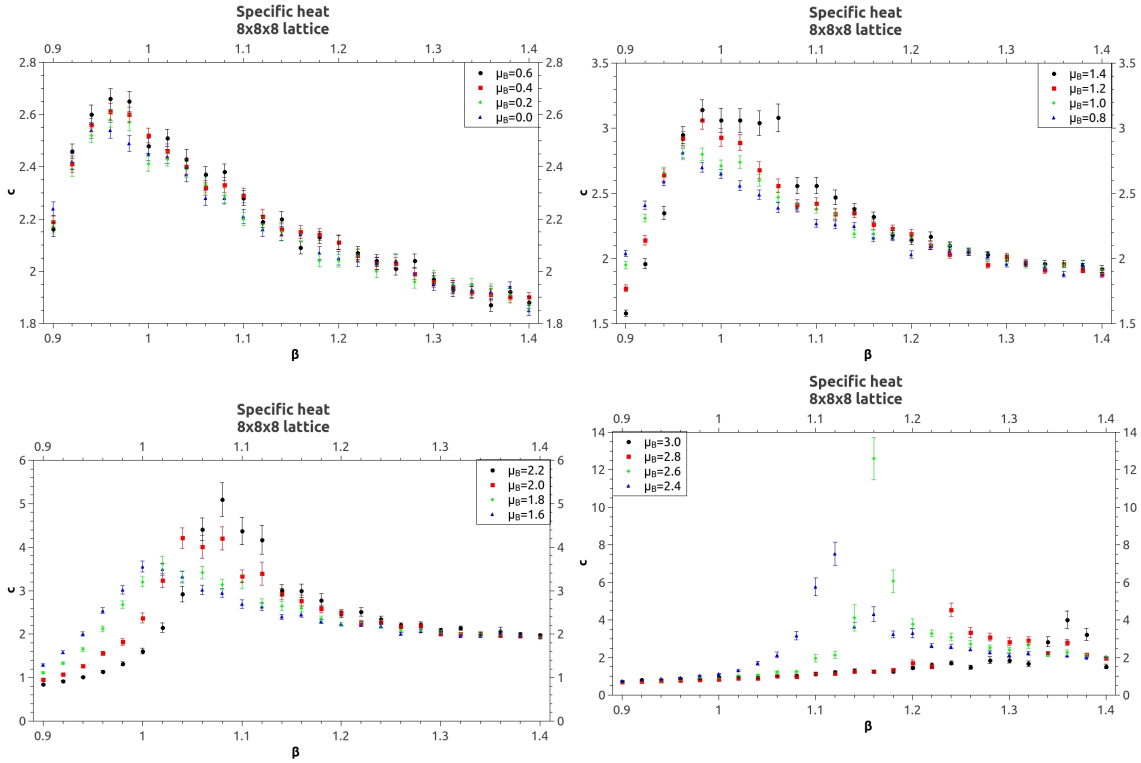

Figure 3.4: Behavior of the specific heat c under several μ_B. The nearly flat behavior around β_c for $\mu_B = 1.4$ may be a hint that this point is near the *critical end point* $\beta_{critical}$: the point where the second order phase transition meets with the first order phase transition.

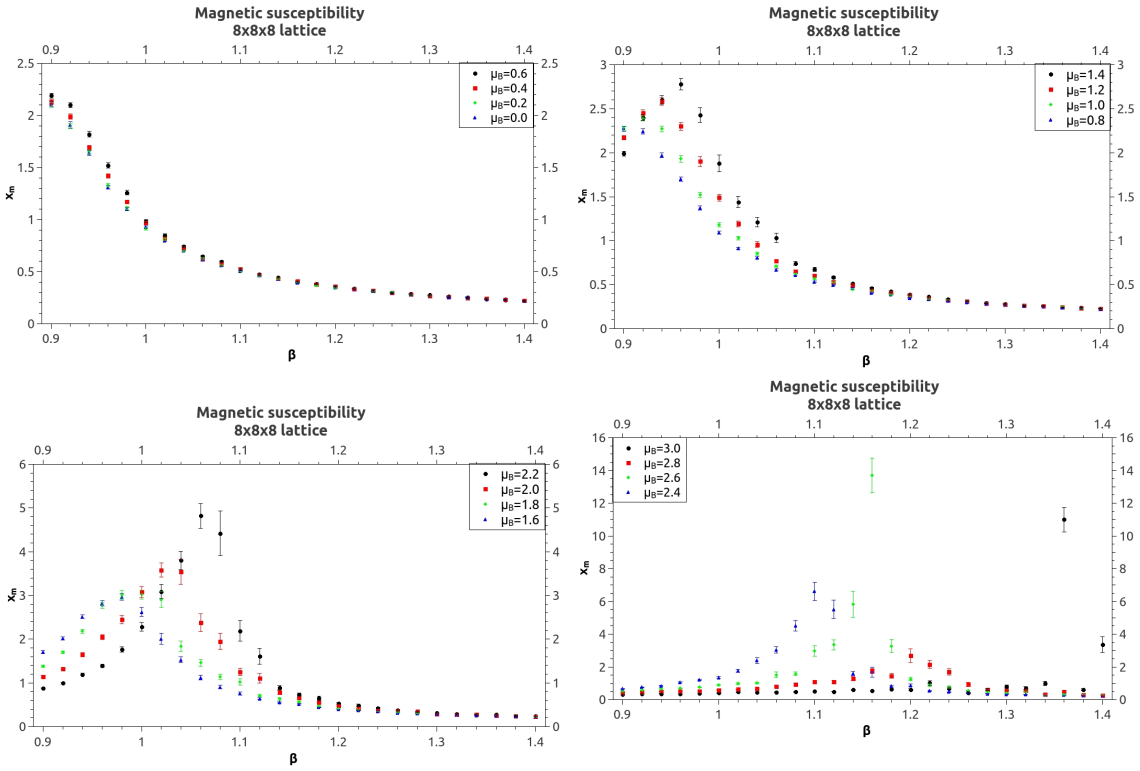

Figure 3.5: Behavior of the magnetic susceptibility. They diverges at β_c but it can be seen a displacement for β_c when it is compared with the β_c obtained from data of the specific heat c.

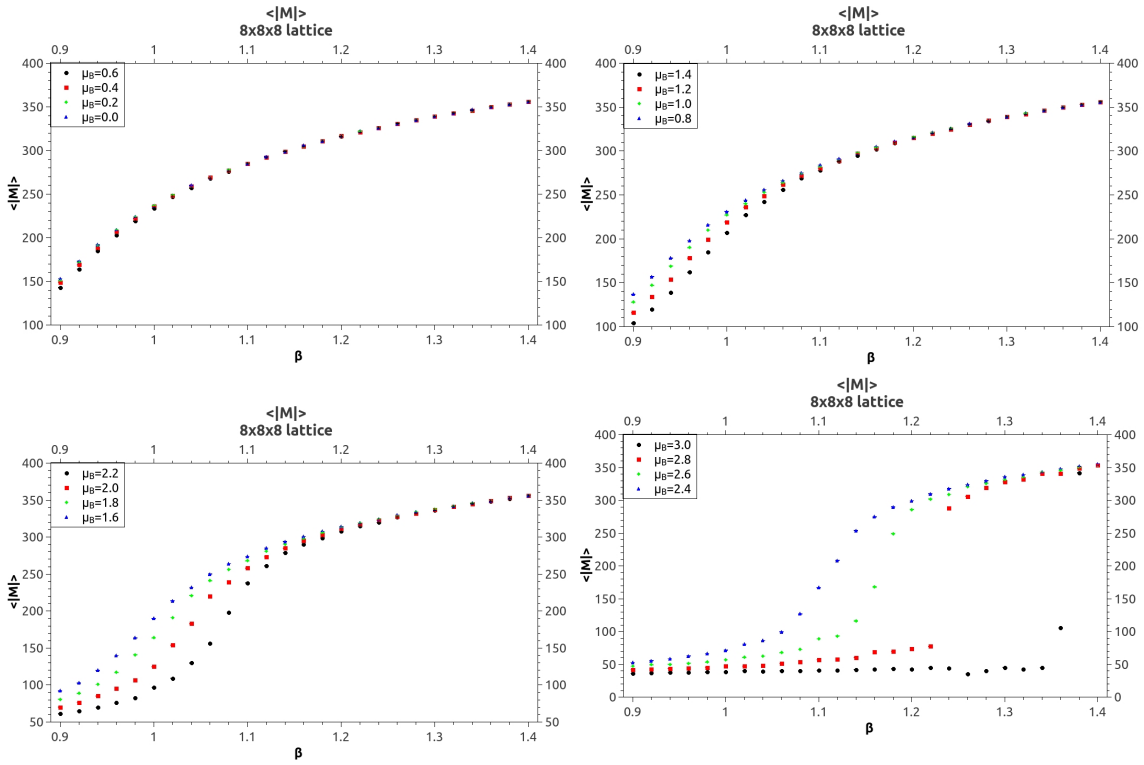

Figure 3.6: Behavior of the order parameter $\langle |M| \rangle$. Due to finite size effects, the first order transition seems like if the second derivative of $\langle |M| \rangle$ were zero. The second order transition seems like a continuous curve with a concavity downward.

Chapter 4

Conclusion

Using the results obtained from $L = 8$, the critical phenomena in each curve for several μ_B was identified and the interval of β was reduced in each case for a test with higher L that took less time and a better resolution. From figure 4.1 it can be deduced that the best data to get the critical curve due to its convergence towards β_c is the specific heat c.

For the values of $\mu_B = 0.0, 0.2, 0.4, 0.6, 0.8, 1.0, 1.2, 1.4, 1.6, 1.8, 2.0, 2.2, 2.4, 2.6, 2.8, 3.0$ the behavior of its thermodynamical quantities near their respective critical behavior were gathered using $L = 8, 12$. To get the extrapolated value of β_c for each μ_B for $L = \infty$ each curve near the critical phenomena of the specific heat c were approximated to a Gaussian fit to get the value of β_c in each case. Using the values of β_c obtained from this method for a specific μ_B and different L, a extrapolation using a linear fit of β_c Vs $1/L$ was used. The value of the intersection of this linear fit with the y-axis is the extrapolated value β_c with $L = \infty$.

Using the method described before, a preliminary critical curve is obtained, as shown in figure 4.2. The preliminary goal of this thesis has been achieved.

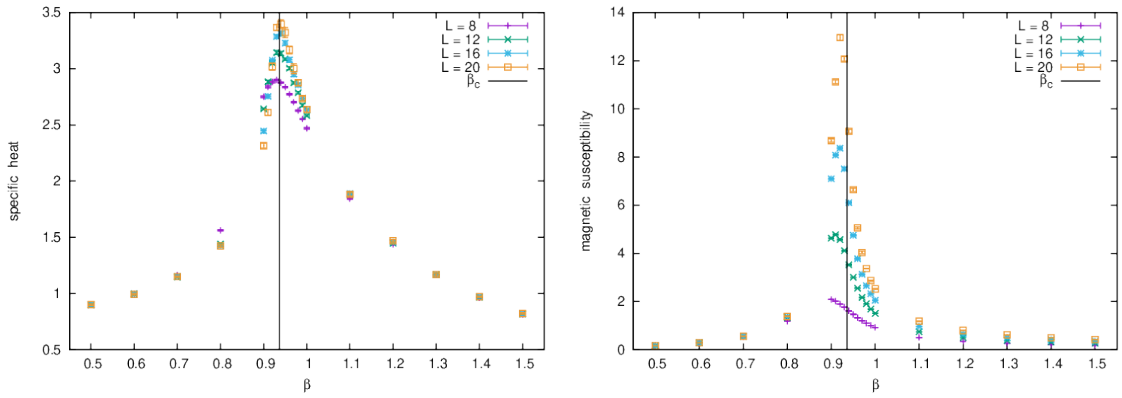

Figure 4.1: Behavior of the magnetic susceptibility χ_m and the specific heat c as L is raisen with $\mu_B = 0$. For both quantities it can be seen that their peaks become higher and narrower as the quantities approaches to β_c. It is remarkable its (interpolated) maximum for c is close to β_c even with a moderate V. The same behavior can be seen for χ_m but its convergence towards β_c is slower.

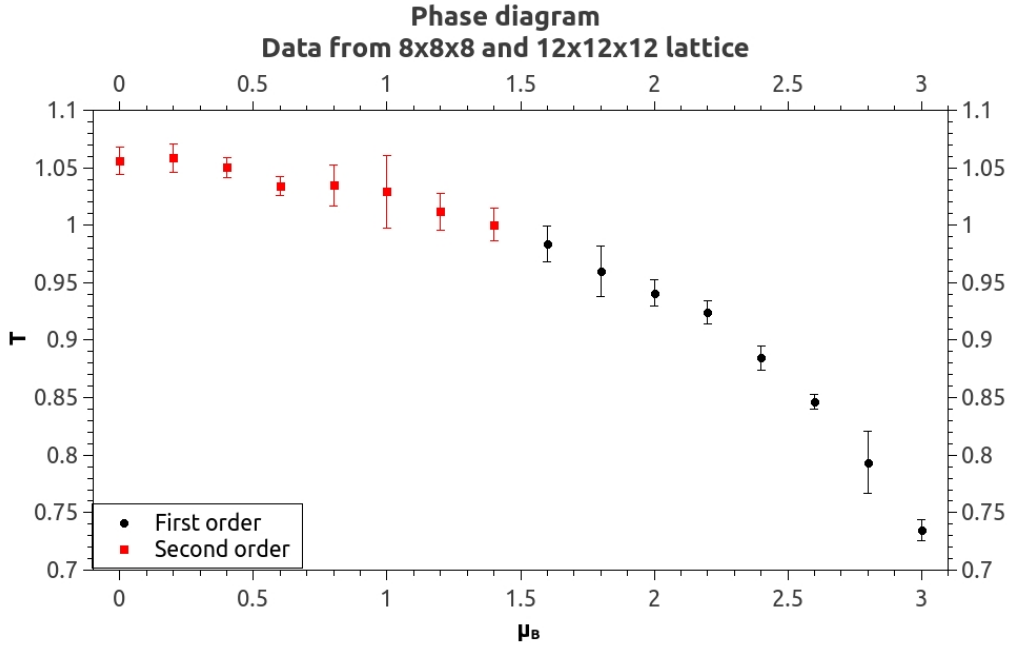

Figure 4.2: Preliminary phase diagram of the σ non-linear $3d$ $O(4)$ model. It shows the order of the phase transition for each point. The *critical end point* was not obtained, but it can be seen it is between $\mu_B = 1.4$ and $\mu_B = 1.6$ with a $\beta_{critial}$ around 1. Observe the likeness with the hypothetical phase diagram from figure 1.1.

Bibliography

[1] M. Creutz, *Quarks, Gluons and Lattices* (Cambridge University Press, 1983). H.J. Rothe, *Lattice Gauge Theories: An Introduction* (World Scientific, 1992). M. E. J. Newman and G. T. Barkema, *Monte Carlo Methods in Statistical Physics* (Oxford University Press, 1999).

[2] M. Bruno, M. Dalla Brida, P. Fritzsch, T. Korzec, A. Ramos, S. Schaefer, H. Simma, S. Sint and R. Sommer 2017 arXiv:1706.03821 [hep-lat]

[3] S. Adler 1969 *Phys. Rev.* **177** 2426

[4] S. Weinberg 1979 *Physica A* **96** 327

[5] R. D. Pisarski and F. Wolczek 1984 *Phys. Rev. D* **29** 338

[6] F. Wilczek 1992 *Int. J. Mod. Phys. A* **7** 3911

[7] K. Rajagopal and F. Wilczek 1993 *Nucl. Phys. B* **399** 395

[8] J. Engels, S. Holtmann and T. Schulze 2006 *PoS LAT2005* 148 arXiv:hep-lat/0509010

[9] F. Basile, A. Pelisseto and E. Vicari 2006 *PoS LAT2005* 199 arXiv:hep-lat/0509018

[10] S. Eijiri *et al.* 2009 *Phys. Rev. D* **80** 094505 arXiv:0909.5122 [hep-lat]

[11] T. H. R. Skyrme 1962 *Nucl. Phys.* **31** 556

[12] I. Zahed and G. E. Brown 1986 *Rept. Prog. Phys.* **49** 825

[13] W. Bietenholz 2010 *Int. J. Mod. Phys. A* **25** 1699

[14] W. Bietenholz 2016 *Int. J. Mod. Phys. E.* **25**

[15] K. P. N. Murthy, arXiv:cond-mat/0104167 [cond-mat.stat-mech]

[16] J. Engels, L. Fromme and M. Seniuch, Nucl. Phys. B675 (2003) 533

[17] U. Wolff 1989 *Phys. Rev. Lett.* **62** 361

[18] B. Berg and M. Lüscher 1981 *Nucl. Phys. B* **190** 412

[19] J. Murakami 2012 *Proc. Amer. Math Soc.* **140** 3289

[20] L. C. Maximon 2003 *Proc. Math. Phys. and Eng. Sc.* **459** 2807

[21] A. P. Gottlob, M. Hasenbusch, Physica A201 (1993) 593.